Investigation of a novel elastic-mechanical wheel transmission under light duty conditions

Yangzhi Chen[1], X. Liu[2*], D. G. Chetwynd[2] and P. Huang[1]

[1]School of Mechanical Engineering, South China University of Technology, Guangzhou 510641, China

[2]School of Engineering, the University of Warwick, Coventry CV4 7AL, UK

Abstract: A novel 'Elastic Engagement and Friction Coupled' (EEFC) mechanical transmission has been proposed recently in which the power is transmitted through elastic tines on the surfaces of the driving and driven wheels. This study introduces new variations of EEFC mechanical wheel transmission (broadly emulating a gear-pair) with small contact areas for use under light duty conditions. Because a drive of this type inevitably has a strong statistical component, theoretical analysis of the geometrical and mechanical relationships has been attempted by using linear modeling and empirical weightings. Several simple forms of the EEFC wheel transmission are tested under limiting (slip) conditions for transmission force and transmission coefficients against normal load. Normalized standard deviation of these parameters is used to summarize noise performance. Models and experiments are in reasonable agreement, suggesting that the model parameters reflect important design considerations. EEFC transmissions appear well suited to force regimes of a few tenths of a newton and to have potential for use in, for example, millimetre-scale robots.

Keywords: Elastic mesh, Friction, mechanical wheel transmission, EEFC

* Corresponding author. Tel:+44(0)24 76523136, Fax:+44(0)24 76418922, E-mail: X.Liu@warwick.ac.uk

Nomenclature

A	contact area between a transmission pair
B	width of contact area
D	transmission, or driving, force
E	elastic modulus of material
F_F	frictional force
F_L	normal load
I	second moment of area of tine cross-section
M	number of rows of tines in the contact area
N_R	number of tines per row
P	force on an individual tine
R	outer radius of wheel
T	torque on wheel
X	half-length of contact area
a	distance between centres or faces
h	height of tine above the base surface
l	distance of contact from fixed end of tine
n	area density of elastic tines
p	engagement probability
r	base radius of wheel
s	distance between base surfaces
t	distance between adjacent rows of tines
x	nominal position of tine from centre-line
α	half-angle of contact area at wheel centre
β	nominal direction of tine from wheel centre
θ	allowable bend angle of an engaging tine
μ	friction coefficient

1 Introduction

A new type of mechanical transmission method has been proposed recently [1], called by its inventors the Elastic Engagement and Friction Coupled, or EEFC, transmission. The EEFC drive can, in principle, be used wherever a friction drive or toothed gear might be feasible. Using mostly elementary Mechanics of Materials [2, 3], a series of basic theoretical and experimental investigations have been reported previously [4-7]. These mainly concerned a highly simplified model of EEFC for flat surfaces with large contact area, such as EEFC belt drive and EEFC clutch drive.

In contrast with the previous work, this study investigates whether such drive mechanisms can be scaled down to millimeter levels for applications in, e.g., medical or other small-scale 'tube-crawling' robots. EEFC drives provide a potential new alternative solution to millimetre-scale drive devices because scaling conventional alternatives introduces serious challenges. Conventional gears become increasingly difficult to make at smaller scales and require critical alignment. Friction drives will be less reliable at small sizes, where the contact forces are low. If such drives themselves become less precise, then simple alternatives may compete on cost-performance even if they are inherently noisy from the statistical nature of their mechanical interactions.

This paper introduces a new variation of mechanical wheel transmission (i.e. one that broadly emulates a gear-pair) based on the EEFC transmission method for use under light duty conditions in millimetre-scale drive devices. After briefly reviewing previous simple analyses, the paper provides an improved model relevant to these conditions. The approximate, mixed theoretical and empirical, model relates the geometrical parameters to the transmission force of the new transmission structure and its related vibration. It then presents some experimental results of the performance (at slip) in order to validate the semi-empirical models.

2 Basic Principles and Structure of the EEFC transmission method

As shown in Fig. 1, the surfaces of the new type transmission pair are covered with arrays of elastic micro- tines. When the two surfaces come into contact, the tines on one surface will interact with those of the counterface surface. This interaction causes a resistance to lateral movement between the two surfaces and can be used to transmit force. The transmission force comprises a friction force between the contacting parts and an engagement force from pairs of elastic tines, hence the name Elastic Engagement and Friction Coupled (EEFC) Transmission [1, 4]. The practicality of creating such

arrays of tines at very low cost is evident from the similarity of the structure shown in Fig. 1 to that of one component of the highly successful Velcro® fixation material.

A previous study [4] has proposed a highly simplified model for the engagement and subsequent sliding of flat surfaces covered with such tines. In essence the model assumes that the tines in contact bend as cantilevers until they slip at some maximum end angle. There is a drag force from this bending (its value depending on the likelihood of engagement) as well as from conventional frictional effects. Hence the transmission or driving force, *D*, is given by [4]

$$D = pnAP_{\max} + F_{\mathrm{F}} \tag{1}$$

where p is the engagement probability, n the area density of elastic tines, A the contact area between the transmission pair, P_{max} the maximum value of load on each tine and F_{F} the maximum (dynamic) value of frictional force. Using simple beam theory [3] for the tines,

$$P_{\max} = \frac{2EI\theta}{l^2} \tag{2}$$

where E is the elastic modulus of material, I the second moment of area at the neutral axis of the cross-section, l is the distance between the fixed end and the contact point on the tine, and θ the angular deflection at that point.

3 Modelling for small EEFC wheel transmissions

3.1 The basic configurations

The EEFC drive can, in principle, be used wherever a friction drive or toothed gear might be feasible. Fig. 2 shows two typical cases for illustration. The first is wheel-to-wheel, as in a classic pair of spur-gear pinions, Fig. 2(a): the EEFC transmission acts as a spur gear emulation (SGE for convenience here). The second case is wheel-to-flat, Fig. 2(b), for gearing between orthogonal shafts as typically found in rack or crown-wheel and pinion drives, bevel gears and frictional wheel drives. It will be referred to here as BGE (EEFC bevel gear emulation). The complexity of the individual and ensemble interactions between tines in these drives makes theoretical analysis extremely difficult and, crucially, casts doubt on the usefulness of such analysis for design purposes. Nevertheless, a semi-empirical model based on gross approximations can help to highlight the relative importance of different parameters. The following discussion is offered for this purpose.

Figs. 3 and 4 sketch the contact area between transmission pairs of the SGE and

BGE modes of the EEFC transmission to identify the major geometrical parameters. For an EEFC transmission with a large contact area and surfaces pressed together (for example, an EEFC belt transmission or EEFC clutch), Eq. (1) might be used for estimating the transmission force [4-7] because all tines experience similar conditions. But for the drives of interest here, the contact area is small and the contact surfaces are significantly curved. The effective engagement length, *l*, for any pair of engaging tines will vary with their positions across the contact area between the transmission pair. Also the relative orientations of tines will vary, as shown in Figs. 3 and 4. Thus, there can be different engagement forces for different pairs of engaging tines, as seen in the sketch of forces for SGE in Fig. 5 (BGE differs only in having one surface perpendicular to the centre-line).

3.2 Geometrical models and parameters

We take it that both surfaces of the transmission pair have tines of height *h*. From Fig. 4, the minimum separation of the base circles is $s = a - r_1 - r_2$ ($s = a - r_1$ in the BGE case), with a design function restriction that $h < s < 2h$. Here, r_1, r_2 are inner (base circle) radi; a， r_1, r_2 and h are the pre-defined geometrical design parameters. Immediately observable features are:

- The area of contact region depends on r_1 and r_2 and can be quite small;
- At the edge of contact region, tines only just touch when undisturbed and so the transmission force fades to zero;
- Pinions may be on relatively rigid shafts so that the centre separation, *a*, is preset, which also presets the nominal overlap of tines, unlike the weight-loaded case in [4] where the gap is taken to settle to approximately *h*.

Taking the SGE case shown in Fig. 3 and assuming, for now, that the tines are rigid, we can determine the maximum angle of contact for each wheel using the cosine rule

$$\alpha_1 = \cos^{-1}\frac{a^2 + R_1^2 - R_2^2}{2aR_1}$$
$$\alpha_2 = \cos^{-1}\frac{a^2 + R_2^2 - R_1^2}{2aR_2} \qquad (3)$$

Where $R_1 = r_1 + h$, $R_2 = r_2 + h$. The length of contact area, $2X$, between points b and c is found from

$$X = R_1 \sin\alpha_1 = R_2 \sin\alpha_2 \qquad (4)$$

For the BGE mode, in Fig. 4, there is a small variant since R_2 and α_2 are undefined and *a*

becomes the distance from the flat base to the centre O_1. This leads to the simpler

$$\alpha_1 = \cos^{-1}\frac{a-h}{R_1} \tag{5}$$

In either case, assuming the narrower wheel has constant width, *B*, the contact area, *A*, between the transmission pair is simply

$$A = 2XB \tag{6}$$

A pair of tines interact at angles β_1 and β_2, which vary in $0\sim\alpha_1$ and $0\sim\alpha_2$ respectively, while their effective lengths l_1 and l_2 vary in $0\sim h$ (or to a lesser range if the wheels do not interlock tines fully along the line of their centres). Then, referring again to Figs. 3 to 5, the geometrical relationship of two interacting tines, can be expressed for the SGE as

$$(r_1 + l_1)\sin\beta_1 = (r_2 + l_2)\sin\beta_2 \tag{7}$$

For the BGE, the right-hand side of Eq. (7) becomes x_2, the distance of the tine from the centre line.

3.3 Wheel geometry and drive torques

Despite the gross simplifications of equations (1) (2), it is reported in [4] that there was reasonable practical agreement with this formula for relatively large flat areas of material and loads of tens of newtons. But, the model clearly has important weaknesses, including:

- The end deflections and angles are too large for the use of simple beam theory;
- As the tines bend, their effective height reduces, so their limiting deflection should depend on the initial separation of surfaces (the experiments in [4] had them pressed together).
- The engagement of hooked tines will generate tension forces that tend to stiffen bending behavior and contribute to the driving, or drag, force.

The drives being investigated here, which have small contact areas between the transmission pair and small transmission forces, are likely to be much more sensitive to the effects neglected in equations (1) (2) than were previously studied regimes.

As shown in Fig. 5, the component of the force, P_y, on any tine tangential to its own wheel contributes to the torque on a lever arm of the appropriate $r + l$. Given the scale of other approximations, it is adequate simply to use *r* for all tines (or, a little more conservatively, *R* for the driving element and *r* for the driven). P_y contributes directly to the linear force on a flat element. The transmission torques *T* are the sum of all these

effects plus that of a friction force F_F, so if there are m rows each containing N_r tines

$$T_1 \approx \sum_{i=1,m}\left((r_1 + l_{1i})P_{y1i} \cdot p \cdot N_r\right) + r_1 F_{\mathrm{F}} \approx r_1\left[\sum_{i=1,m}\left(P_{y1i} \cdot p \cdot N_r\right) + F_{\mathrm{F}}\right]$$
$$T_2 \approx \sum_{i=1,m}\left(r_2 + l_{2i})P_{y2i} \cdot p \cdot N_r\right) + r_2 F_{\mathrm{F}} \approx r_2\left[\sum_{i=1,m}\left(P_{y2i} \cdot p \cdot N_r\right) + F_{\mathrm{F}}\right] \quad (8)$$

The deflection of the elastic tines has been ignored on the assumption that it has only a small impact on these geometrical relationships (for illustration, note that a simple circular arc reduces tine height by less than 15% even for an end deflection angle θ of 1 rad.). For BGE mode, T_1 will be as in Eq. (8) but alternative situations arise for element 2. If the emulation is of a rack and pinion or linear friction wheel drive, the output is directly a force, D_2, found as in Eq. (8) but without including the radius (lever) terms. In cases emulating perpendicular rotations (bevel gears, crown wheels, *etc*.) D_2 is manifest on the flat of the wheel, and the output torque is its product with the average distance of contact area from the axle of that wheel.

The number of tines in the contact area of a transmission pair can be calculated from the known geometrical parameters of the elastic tines and values of α_1, α_2 and X obtained by Eqs (3)-(5). However, Eqs (3-5) and (7) are not sufficient to uniquely determine l_1 and l_2 for each transmission pair. Hence, neither can the P_y terms be estimated. One further relationship between β_1 and either β_2 or x_2 is required. A difficulty arises because a tine on one wheel might be able to meet tines from two rows of the other wheel, especially if the tines are fairly long compared to the space between them ($h > t$). It can be resolved by an additional assumption, quite minor compared to some made previously, that there is a fixed ratio between β_1 and either β_2 or x_2 equal to the nominal gear ratio of the wheel speeds. This is justified by observing that a pair of interacting tines at the centre of the contact region are effectively parallel and then move away from each other according to the speeds of the wheels.

3.4 Modelling tine engagement forces

With the engagement probability providing an empirical factor to tune the model, approximations that do little more than identify the form of relationships between parameters will be used to estimate the forces P_{y1} and P_{y2}. As well as the hooked tines considered in previous work, straight tines will be considered in this study. We take wheel 1 as the driving element and wheel (or flat) 2 as the driven element, whenever it is necessary to distinguish them.

Consider two straight cylindrical and parallel tines, one pushing against the other. They will bend away from each other and, since the contact vector will not generally align to the drive direction, this allows the driving tine to slip by the driven one. The tines are approximately cantilevers loaded by equal and opposite point forces acting at the mid-point of their overlapped region. The tine overlap depends on the gap width, $s(x)$, which can be approximated by a quadratic function, taking it as h at the centre (it is an easy modification to account for wider central gaps). The effective tine length is then

$$l = s(x)/2 = h\left(1 + \left(x/X\right)^2\right); \qquad |x| \le X \tag{9}$$

An estimate for the typical maximum force is that it occurs when each tine of a pair deflects by $d/4$ at the contact point. This yields

$$P_y(x) = \frac{6EId}{h^3}\left(\frac{h_0}{s(x)}\right)^3 = P_{y0}\left(\frac{h}{s(x)}\right)^3 \tag{10}$$

Technically this force, relating to the deflection needed to clear an initial misalignment of $d/2$ between axes, acts at an angle to the drive direction, but this is here ignored in a crude reflection of the increasing ratio of friction to direct pushing as deflection progresses. At this level of modeling approximation, the common force at the contact point, Eq (10), is taken also to represent the normal force to each tine, P_{y1} and P_{y2} (although not physically correct), because the weighting in Eq. (9) concentrates the effort strongly onto the most nearly parallel central tines. The probability of engagement of straight tines will depend on local conditions, but a major factor will be the amount of clear space between tines, which is summarized by the ratio of diameter to spacing, d/t.

Hooked tines could experience an interaction similar to that proposed for straight ones. However if the hooks of a pair engage, the force will be by drag as the tines exit, with disengagement governed mainly by a critical degree of bending. The critical angle could be thought of as either a combined value from both tines or the larger of the individual ones (these were essentially the same for the previous symmetrical flat-to-flat model [4]). Since the driving tine is earlier in the causal chain, its tangential force and deflection can never be the smaller. Taking disengagement as happening when this tine bends though an angle equivalent to that included by the hooked end, the maximum force on the driving tine P_{y1} is simply that given by Eq. (2). However, because the drive is likely to be significant near the exit region, the orientation cannot be ignored. The

force nominally perpendicular to the driven tine will be the component

$$P_{y2} = P_{y1}\cos(\beta_1 + \beta_2) \tag{11}$$

Hooked engagement is very unlikely in the entry regions of the contact zone, when tines tend to be sliding towards each other. It is highly likely in the exit region as tines slide apart. There is, therefore, a case for modeling the total effect as a mixture of the two interaction modes. For example, it might be assumed the all tines from the entry to the centre behave as if straight, modeled by Eq. (10), and all the rest as if hooked, modeled by Eq. (11). This idea is explored further in section 5. Since the hooked ends occupy most of the space between tines, the engagement probabilities for both modes will be much higher than for truly straight tines, probably approaching unity.

The approach used to derive Eqs (9) to (11) provides a plausible overview of the major mechanical interactions but it hardly constitutes a reliable or accurate model and more basic studies of models are in progress.

4 Testing of transmission performance

4.1 Test-rig

The transmission characteristics of the EEFC wheel transmission were tested using a custom-built test-rig designed for small-scale frictional force measurement [8, 9]. Fig. 6(a, b) show a photograph and schematic diagram of the apparatus. It comprises a small rotating disk (wrapped with specimen 1) driven by a DC motor with a gear box (135:1) and a tachometer, and a sample holder (carrying specimen 2) attached via a load cell to a flexure type spring mechanism with a capacitive displacement sensor. The load cell measures the loading force and the capacitive sensor measures the frictional force. As illustrated in Fig. 6, the upper specimen rotates about a horizontal axis to generate sliding motion against a static lower specimen. The normal load between the specimens is provided passively by a ball-bearing supported lever carrying a sliding weight. Once the counterweight is clamped in position, it produces a nearly constant pre-set static contact force, as long as the lever remains roughly horizontal. The lower specimen is attached to the lever through a vertical-axis strain gauge load cell and then a stiff horizontal linear flexure mechanism. The load cell provides continuous monitoring of the actual normal load, while a high-sensitivity capacitive gauge measures the flexure displacement and hence the friction force while minimizing lateral specimen motion. The apparatus is operated automatically by a PC and a data acquisition system, based on

LabVIEW® and MATLAB® software packages, to provide real-time measurements of the loading force, frictional force, and dynamic friction coefficient of the specimen under test. Both force sensors were calibrated by standard weights and the nonlinearity is well within 1% for the range used in this work. The loading force can be set at up to 3 N, the friction force range is 2 N and both forces are resolved to better than 0.1 mN with small thermal zero drift and low spurious vibration [8, 9].

4.2 Preparation of Specimens

Standard Velcro® products available commercially are unlikely to offer optimal surface structures for EEFC devices. Nevertheless, their ready availability makes them highly convenient for testing the basic ideas. The upper, type 1, specimen is a mild steel disc, 20.4 mm in diameter and 8.5 mm in width, with Velcro® glued around its complete periphery. Normal Velcro® tines are hooked at the free end and effectively arranged in pairs along fairly straight rows. 'Straight' tines were produced by gently cutting the ends from normal ones. Five different type 1 specimens involved either just a single tine or one, two or three pairs in rows along the axial direction. Table 1 gives details of these arrangements. In all cases, the spacing, *t*, between the rows was 0.8 mm and the tine diameter was 0.15 mm. The lower, type 2, specimen is simply a 22 mm diameter circular Velcro® pad, which is glued to the flat surface of a thin steel plate fixed on the load cell of the test-rig. With this specimen pair, the test-rig measures the limiting (slip) conditions for an EEFC emulation of a rack and pinion (BGE mode).

4.3 Experimental procedure

For each pair of specimens, the normal loading force and the drag force were recorded simultaneously while the wheel slipped against the fixed counter-face. The free rotational speed was about 35 r.p.m., giving a sliding speed of around 35 mm s^{-1}. The drag force represents the maximum transmission force of the particular EEFC system. Real-time information is given on the load, drag force and instantaneous transmission coefficient (the ratio of these forces). Other functionally important parameters and averages can be calculated off-line from the recorded time histories.

Loading force is expected to influence especially the friction-generated component of the transmission force, transmission coefficient and transmission power, so tests were made over a range of static loading forces (up to about 1 N) set by moving and fastening the sliding weight on the lever. In this mode of operation, the specimens float together, with the assumption that their tines merge to almost their full depth in the

centre of the contact region, that is the initial gap between two surfaces was set to be approximately *h*. This is experimentally convenient because rotational errors from the type 1 specimen have negligible effect on the forces and engagement depths provided speeds are low enough to keep inertial forces small. However, practical designs are more likely to involve fixed bearings for both elements of an EEFC drive. Thus, some tests were performed in which the surfaces were first brought together normally and then the lever arm locked into that position by a screw before the drive was started.

Since EEFC transmission derives from individual contacts making and breaking, relatively high noise levels are expected. Generally, therefore, time averaged parameter values are appropriate to represent useful behavior. Transmission coefficient can be considered either by time averaging the instantaneous ratios of the forces or by taking the ratio of the average forces. The latter is considered more stable, but both were evaluated. The magnitude of the noise was estimated in terms of the standard deviation of a signal normalized by the mean value for that signal. This approach is satisfactory for random noise distributions not too far from Gaussian and for periodic components.

Because the tines are distributed in a fairly regular rectangular array across the surfaces, the pitch of the tines in the direction of drive varies with their orientation to it. The relative alignment of the arrays on the two interacting surfaces might affect the transmission force. Therefore, a preliminary experiment compared the average transmission loads when the type 2 specimen was fixed at relative angles of 0°, 45°and 90°. Fig. 7 shows that there is no clear effect from orientation for the single tine case (noise levels and significance are discussed section 4.4). Other patterns of tines showed more variation in specific tests but there was still no consistent pattern. Orientation seems not to be a practical problem, certainly within the scatter about design data we expect of these devices, and further testing was executed almost entirely in the 0° relative orientation.

4.4 Test results and discussion

Dynamic measurements of loading force, transmission force and transmission coefficient (the instantaneous ratio of transmission force to loading force) are recorded directly by the LabVIEW® control program. Fig. 8 shows a typical set of records plotted using MATLAB®. 500 data points (sampled at equal time intervals) were taken over 50 s for a type 1 specimen having 3×2 straight tines at relative angle 0° under a nominal static loading force 0.4 N from the floating stage. The variability of the contact

between the tines leads to large rapid fluctuations of the forces about their means, which feeds back into the loading force. The dynamics of the spring mechanism cause the measured transmission force to become negative on rare occasions. The instantaneous transmission coefficient can be subject to rare, extremely high values because, through inertia, the loading force might instantaneously be close to zero while the transmission force retains a significant value. The averaged transmission coefficient (defined as the ratio of averaged transmission force to averaged loading force) is more stable and has value 1.91 for the data shown in Fig. 8.

Fig. 9 summarizes the force transmission capabilities of all the tine patterns tested (at 0° orientation). The graphs are truncated at higher loads when the transmission force sometimes exceeded the 2 N maximum of the sensor. At smaller loads, the average transmission force increases rapidly with average loading force and considerably exceeds it. The number and shape of tines on the type 1 specimens have an important, non-uniform influence on the average transmission force. For example, with loading force preset to 0.2 N, the average transmission force is, in rank order, 0.5 N for 3×2 straight tines, 0.74 N for 1 tine, 0.86 N for 2 tines, 1.06 N for 3×2 tines, and 1.21 N for 4 tines. It was generally found that increasing the number of tines in a row had a diminishing beneficial effect, except that the 2x2 tine arrangement consistently gave the best performance. This could be a statistical freak but it might indicate that at very small loads additional tines contribute more to inefficiency through the imperfect geometry of the wheels than they do to the useful drive. In any case, it appears that one or two tines per row are adequate for the anticipated applications in micro-robots. The straight tines show a lower and straighter curve, consistent with a smaller proportion of engagement drive relative to friction drive, as would be expected.

The relative effects of engagement and friction processes show more clearly in the transmission coefficients. Fig 10(a) plots the averaged transmission coefficient against averaged loading force. For all five specimens, it is large at small loading forces, but settles back as the load increases. At 0.4 N it is around 2.0 for specimens with 1 tine, 1x2 tines and 3x2 straight tines, after which it deceases only slowly. The instantaneous transmission coefficient fluctuates so much that even its time average leads to large and inconsistent values at small loads, although there is a similar overall trend to that of the averaged coefficient. In practice, the inertia of a real drive would ‘clip’ the extreme values, so it is more sensible to delete outliers before averaging the instantaneous transmission coefficient. Fig. 10(b) shows the result after removing all values greater

than 3σ from the mean (about 5% of points removed).

The profiles in Fig. 8 suggest that standard deviation (STD) is useful for summarizing noise in the force measurements. The distribution of the transmission coefficient signal is less amenable to summary by a single number and will not be discussed here. Fig. 11 shows how the normalized STDs of the loading force and transmission force vary with the average loading force. Normalization is always by the mean value for the particular data set in order to express the relative importance of the noise. The normalized STD of the loading force decreases rapidly as the load increases up to about 0.3 N, decreasing more slowly as the average loading force increases further. The trend is very consistent with all samples, reaching rather less than 0.5 at moderate loading forces. The normalized STD of transmission force decreases very rapidly to about 0.5 or less as the average loading force rises from zero but stabilizes to a very slow decline at loading forces above 0.3 N for those specimens with 1 tine or 2 tines, with slightly higher values for 6 straight tine specimens.

Taking all these results together, a key finding is that a loading force 0.3~0.4 N is a good working condition for all the major factors in an EEFC structure (BGE) with 1-tine, 2-tine or 6-straight tines made from standard Velcro® products. The data shown, and other results, suggest that the drives have typically higher transmission coefficients at small loads but that actual behaviour is more variable and unpredictable (in a design sense). Much smoother behaviour is found when the loading force exceeds about 0.3 N. Transmission coefficients continue to fall slowly with increased loading force, within the ‘stable’ region, but generally remain above unity. A type of EEFC transmission structure made from 2-tine standard Velcro® has been applied recently to a novel device for driving a micro-robot for use within tubes [10]. It is worth noting that this recommended working condition is for the chosen type of tines. For other types of tines, in terms of materials and shapes, further tests are needed to search for the optimal working conditions.

All results discussed so far were taken with the loading lever in its floating condition. An extensive set of comparison tests between floating and locked conditions was also performed. The surfaces were brought together so that the tines interacted strongly (sometimes with a deliberate preload from the lever counterweight) before the lever position was locked. This more closely represents the situation of a drive supported in relatively rigid bearings. The results were compared both to tests under the same, but unlocked, initial conditions and to the whole body of floating tests.

Test-to-test variability was even higher than previously and no consistent, strong patterns were found, although there were general tendencies that appeared consistent with previous observations. The locked condition tends to give higher averaged loading force compared to nominal and higher averaged transmission force and transmission coefficients, although still within the general ranges shown in Figs 9 and 10. Noise (as normalized standard deviation) and variability were generally higher on locked tests. The majority of locked tests involved small nominal load forces in which region the floating loads also result in more variability and occasionally very strong transmission characteristics, but there seems to be also some extra effect from the locking. One possible explanation could be that geometrical errors lead to a varying gap wider than the nominal h when running between centres, leading to poorer and more erratic (lower probability) engagement. The way in which forces from tine interactions feed back into the loading force may also be affected by locking.

Overall, the general trends are similar in all the experimental schemes and with all the tine combinations tested. The best compromise between design predictability, high averaged transmission coefficient and introduced noise lies always with a loading force in the region of 0.4 N. It appears slightly 'better' to have a floating design rather than one between fixed bearings, but practical designs might still prefer the latter. The 'noisy' region below 0.3 to 0.4 N loading may be less attractive, but can offer high transmission coefficients for situations that can tolerate it, e.g. driving a flywheel.

5 Comparison between model estimates and experimental results

The experimental conditions correspond to a BGE model with $r_1 = 10.2$ mm. The intention is that tines overlap completely in the middle of the contact zone, so it is assumed that $a = R_1$. For the Velcro® material used, tines have a diameter $d = 0.15$ mm and, assuming a constant circular cross-section, the second moment of area of the section is $I = 2.48\times10^{-17}$ m^4. The rows are spaced at $t = 0.8$ mm. The height, h, is given in Table 1. The values reported in [4] are used for elastic modulus, $E = 3\times10^9$ Pa, maximum angle of bending for hooked tines, $\theta = 1.05$ rad, and estimates for friction coefficient, $\mu = 0.35$, and engagement probability, $p = 0.7$~1.0. The latter two parameters are less obviously relevant to the different conditions of the current tests. For straight tines, basing the probability on the ratio d/t gives $p \approx 0.2$.

For a contact region with tines as shown in Fig.4, substituting above values of a, h

and R_1 into Eqs. (5) and (4), we have $\alpha_1 = 29.4°$ and $2X = 11.46$ mm. Comparing $2X$ to t indicates the number of rows of tines in the contact area between the transmission pair to be $m = 15$.

From Eqs. (9) and (10), for a central tine, X=0, we have $l = \frac{h}{2}$ and $p_y(x) = p_{y0}h^3$. Substituting the values of E, I, d, h, l, θ into Eq. (10), for 'straight' contact, gives the force as $P_{y0} = 0.02$ N; for hooked interaction, Eq. (2) gives the force as $P_{y1} = 0.07$ N. Following the proposal in section 3.4, we assume straight interaction up to the centre and hooked interaction from thereon. Substituting Eq. (11) into Eq. (8), the total transmission force for hooked interactions reduces to fixed factors with a weighting depending on a sum of cosines. Taking the tines as symmetrically placed within the contact region at equal steps in β_1, the weighting depends on the sum of (cos4.2°, cos8.4°, … cos29.4°). Always $\beta_2 = 0$ for the BGE configuration used in the experiments. Similarly, substituting Eq. (10) into Eq. (8), the total transmission force for straight contacts reduces to fixed factors with a weighting depending on summing purely geometrical terms from Eq. (8) and (10) using symmetrical equally divided steps in x/X, in sevenths for the present case. Then, Eq. (8) gives the predicted transmission force as

$$D_2 = (6.63P_{y1} + 3.37P_{y0})pN_R + \mu F_L \qquad (12)$$

where, F_L is the normal load on the contact region. If we assumed that all interactions are hooked or all straight, the bracketed term becomes $14.26P_{y1}$ or $7.74P_{y0}$, respectively.

It is clear from Fig. 9 that the transmission force does not rise linearly with N_R. With practical tolerances and misalignment, once there is a full engagement of a pair of tines it seems unlikely that other pairs in the same rows will be able to exert their full potential. From this viewpoint, it makes sense that there is a particularly small improvement of a single pair over a single tine. The probability factor will need to be scaled (non-linearly) according to N_R. The curves settle to steady slopes that suggest the friction term is larger than was previously reported. Table 2 indicates values for the unspecified parameters in Eq. (12) that give a sensible match to the experimental curves at three functionally interesting loads. All the values are in reasonable ranges: probability decreases with N_R and friction coefficient is 0.6 to 0.7. If this modeling approach has any validity, a mixed version such as Eq. (12) appears clearly superior to

assuming all interactions are of the same type. Using the model as a guide, of the order of 60% of the transmission force arises from tine interaction and 40% from direct friction for the ‘best’ operating load of about 0.4 N.

The semi-empirical models introduced in section 3.3 propose a fixed interaction term and a linear friction term. The experimental curves suggest that the force tends to a linear relationship equivalent to a coefficient of friction as the loading force increases. The curved behavior at low loads probably arises because in a floating configuration the tines do not mesh effectively until there is a sufficient force to push them together. Thus, the average depth of engagement reduces below some critical load, leading to a smaller contact region, weaker interaction forces and lower engagement probability. If this is the case, it would be expected that the critical load would increase with the number of tines, as is seen in the relationship between the range of the curved section and N_R in Fig. 9. This effect could be modeled, perhaps by a piecewise linear fit, but, given the number of accumulating approximations, it will not be pursued here.

The contact region with the shorter straight tines has $\alpha_1 = 24.4°$ and $X = 9.26$ mm leading to $m = 11$. The modeling parallels the straight contact part of that just discussed, except that the steps in x/X are in fifths. Eq. (12) still applies except that the bracketed term becomes simply $5.56P_{y0}$ and now $P_{y0} = 0.07$ N. For $N_R = 6$, a good fit to the experimental data of Fig. 9 is found with $p = 0.15$ and $\mu = 0.75$, when for loads of 0.2, 0.4 and 0.8 N, the transmission forces are predicted as 0.51, 0.66 and 0.96 N respectively. Model and experiment both show a much greater contribution from friction drive when hooks are absent.

6. Conclusions

The limiting slip behavior of a novel EEFC wheel transmission under light duty (preset loading force is below 1N) has been studied by semi-empirical modeling and experiment. The statistical nature of the contact between arrays of meshing tines ensures that the drive characteristic is always noisy but the EEFC can be effective and may have some advantages over traditional mechanical transmissions for driving small mechanical systems such as free-crawling micro-robots intended for applications within tubes. It can be smaller, lighter in weight, lower in cost and easier to assemble than conventional transmissions.

In this study the active surfaces were of standard commercial Velcro® material in

a configuration emulating a rack and pinion or linear friction drive. With straight tines there is a modest increase over friction through direct contact forces. Hooked tines can link to each other, providing an additional type of transmission, which is the largest effect under most conditions studied. The ‘best’ working condition, balancing between noise levels (measured as normalized standard deviations of the time-varying forces), loads and transmission forces, has an average nominal load of 0.3~0.4 N for all patterns of tines. The average transmission force is then about twice the nominal load. It appears that arrays with just one or two tines in each row can produce sufficient transmission force and power to drive a useful micro-robot system, with a diminishing benefit from using more. The relative orientation of the arrays of tines on the two surfaces has little effect on behavior, an important feature because orientation varies with rotation when using EEFC to emulate commonly occurring equivalents of bevel gears.

Although this work used commercially available Velcro® material (which was also used in some prototype mechanical systems), custom designed sets of tines are likely to provide even better performance. The EEFC concept offers an effective alternative design approach for a range of small scale applications. Practical and theoretical investigations of other geometrical forms are in progress.

Acknowledgments

The Project sponsored by the Natural Science Foundation of Guangdong Province (05006497) and SRF for ROCS, SEM. The authors would like to thank for their support academic and technical colleagues in the MEMS Research Group at South China University of Technology and the Microsystems Technology Cluster at the University of Warwick.

References

[1] Huang Ping, Chen Yang-zhi, Zhu Wen-jian, Wang-Tao, Cui Han-sheng and He Jun, Elastic engagement and friction coupled transmission method, Chinese Patent, Application. No. 98107195.3, 1998

[2] Motts, R. L. Applied Strength of Materials. 3d ed. Upper Saddle River, NJ: Prentice-Hall, 1996.

[3] Popov, E. P. Engineering Mechanics of Solids. Upper Saddle River, NJ: Prentice-Hall, 1990.

[4] Huang P., Chen Y. Z., Zhu W. J. and He J., Study on the elastic engagement and friction coupled transmission, Proceedings of the International Conference on Mechanical Transmissions. Chongqing, China, 283-287, 2001.

[5] Chen Yang-zhi, Huang Ping, and He Jun, Dynamic experimental study on Elastic engagement and friction belt transmission, Chinese Mechanical Engineering, Vol.8, 901-902, 2000.

[6] Chen Yang-zhi, Huang Ping, Deng Bing-yu and Chen Zhi-bing, Test-rig for the performance testing of clutch coupled with elastic engagement and friction, Chinese Patent, No. ZL 002 39567.3, 2000.

[7] Chen Yang-zhi, Huang Ping and Xu Luo-hua, Theoretical analysis on the belt transmission coupled with elastic engagement and friction, Journal of South China University of Technology, Vol.29, pp.47-50, 2001.

[8] Shen Zhi-qian, Investigation on surface and surface friction behaviour of welding wires, MSc dissertation, School of Engineering, The University of Warwick, UK. September 2003.

[9] Liu X., Chetwynd D. G., Gardner J. W., Smith S. T., Bartlett P. N. and Beriet C., Measurements of tribological properties of polypyrrole thin film bearings, Tribology International, 31 (6), 313-323, 1998.

[10] Chen Yang-zhi, Chen He-en, Huang Ping and Zhang Jian-wei, The methods and device of single-wheel direct driving for micro-robot for in-tube, Chinese patent, No.03113927.2, publication number: 1438167, 2005.

Figure and Table Captions

Fig. 1 The surface structure of the new EEFC transmission pair.

Fig. 2 Sketches of two EEFC wheel transmission arrangements, (a) a spur gear emulation, SGE, and (b) a bevel gear emulation, BGE.

Fig. 3 Sketch of the contact region and geometrical parameters for the EEFC transmission in SGE mode.

Fig. 4 Sketch of the contact region and geometrical parameters for the EEFC transmission in BGE mode.

Fig. 5 The action forces of a tine pair (SGE mode), showing (a) the active engagement and (b) free-body force analysis.

Fig. 6 (a) Photograph and (b) schematic representation of the friction test apparatus.

Fig. 7 The effect of orientation of tine arrays on the averaged transmission force.

Fig. 8 A typical set of raw time series data obtained from the friction apparatus: (a) loading force,
(b) transmission (drag) force, and (c) the instantaneous transmission coefficient.

Fig. 9 The average transmission force as a function of the average loading force

Fig. 10 Transmission coefficients as a function of averaged loading force: (a) averaged transmission coefficient (ratio of time averaged forces), and (b) time average of instantaneous transmission coefficient after removal of outliers.

Fig. 11 Normalized standard deviation of (a) loading force and (b) transmission force as a function of averaged loading force.

Table 1 Parameters of Velcro® surfaces used for different type 1 specimens.

Table 2 Comparison of transmission forces for hooked tines estimated from experimental data in Fig. 8 and from predictions using Eq. (12). Values in brackets are extrapolations.

FIGURES AND TABLES

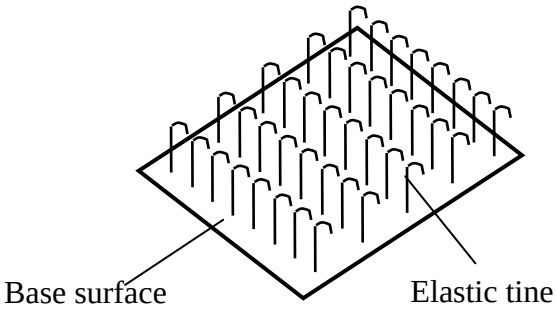

Fig.1 The surface structure of the new EEFC transmission pair

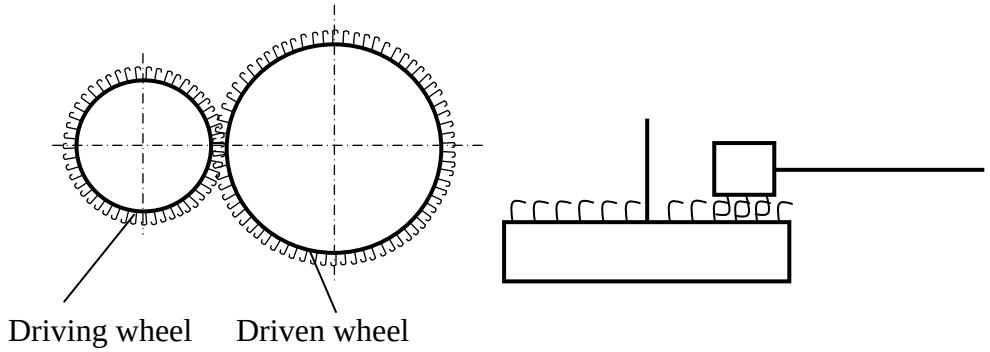

Fig. 2 Sketches of two EEFC wheel transmission arrangements, (a) a spur gear emulation, SGE and (b) a bevel gear emulation, BGE.

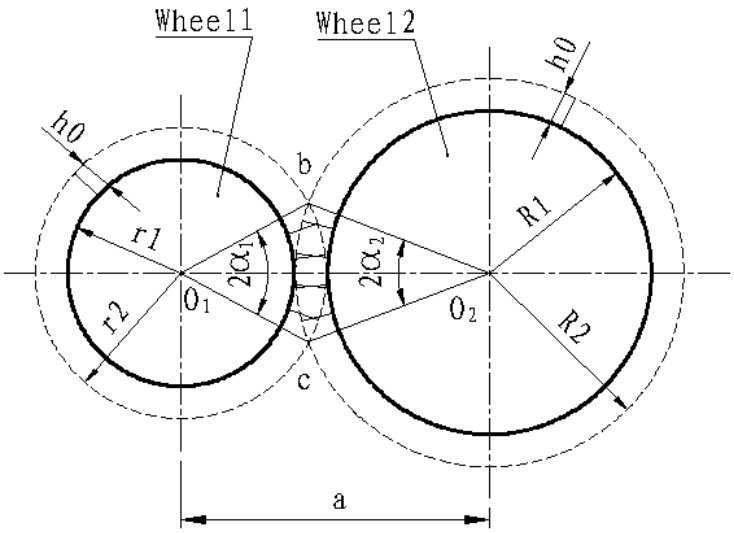

Fig. 3 Sketch of the contact region and geometrical parameters for the EEFC transmission in SGE mode.

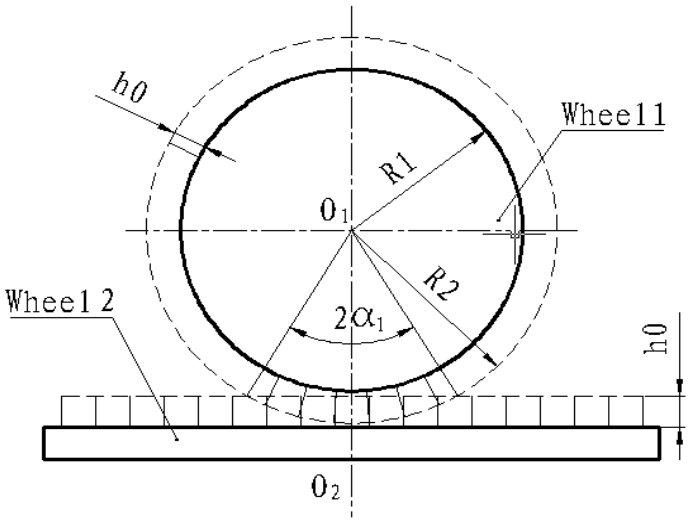

Fig. 4 Sketch of the contact region and geometrical parameters for the EEFC transmission in BGE mode.

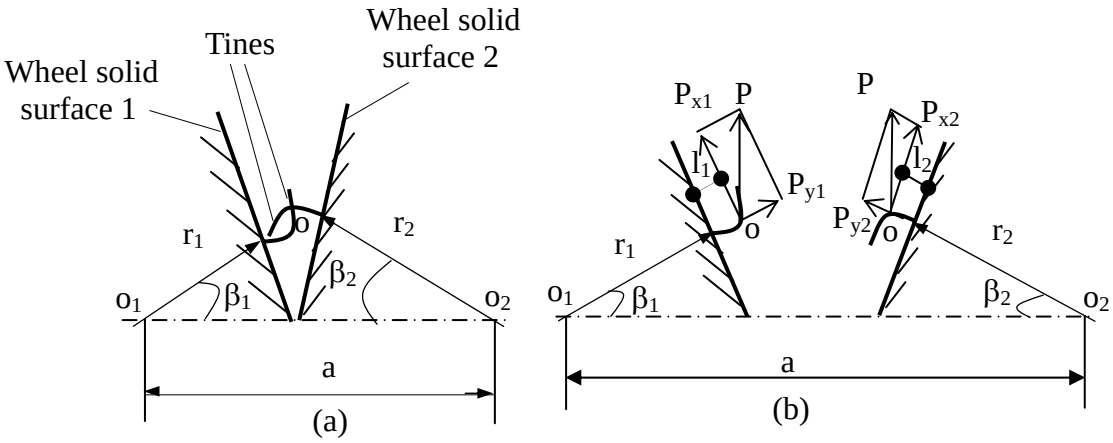

Fig. 5 The action forces of a tine pair (SGE mode), showing (a) the active engagement and (b) free-body force analysis.

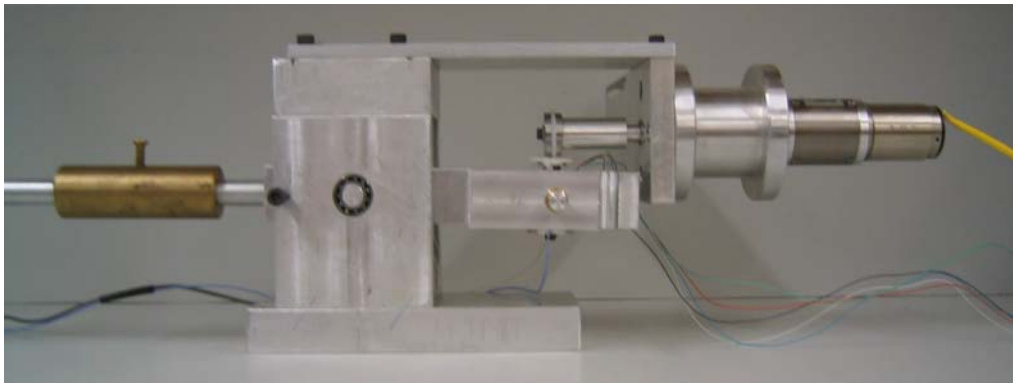

(a)

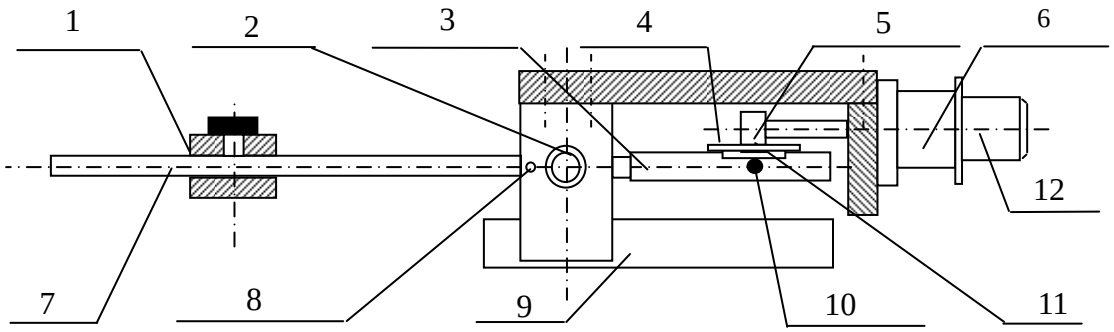

(b)

1- Counterweight 2-Pivot point 3-Spring flexure 4-Specimen 2 5-Specimen 1 6-Gear box 7- Lever 8-Scew 9- Base 10-Pricision sensor 11-Load cell 12-DC motor

Fig 6 (a) Photograph and (b) schematic representation of the friction test apparatus

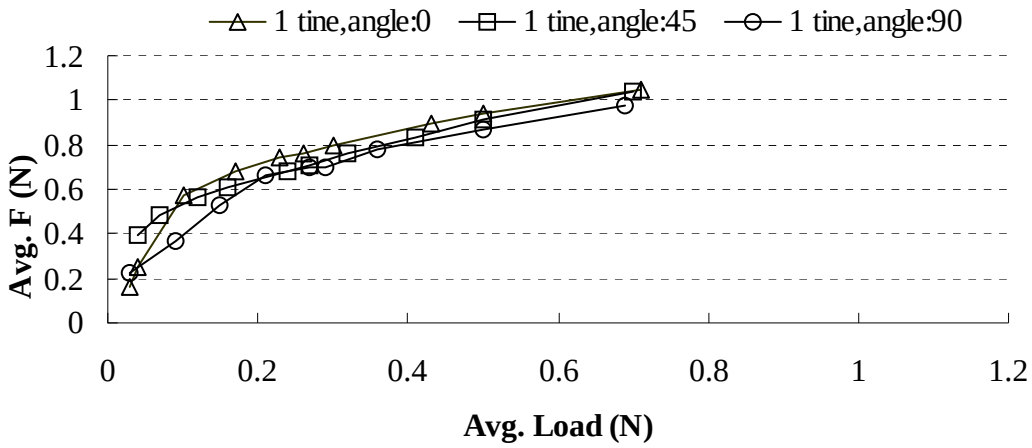

Fig. 7 The effect of orientation of tine arrays on the averaged transmission force

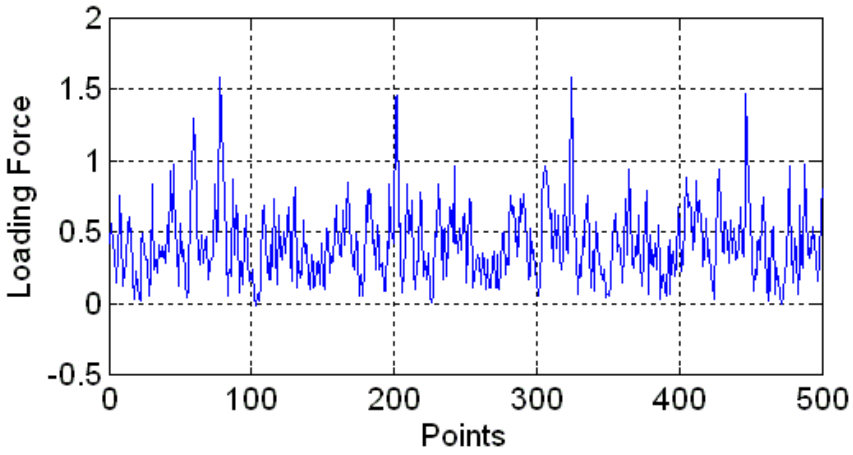

(a)

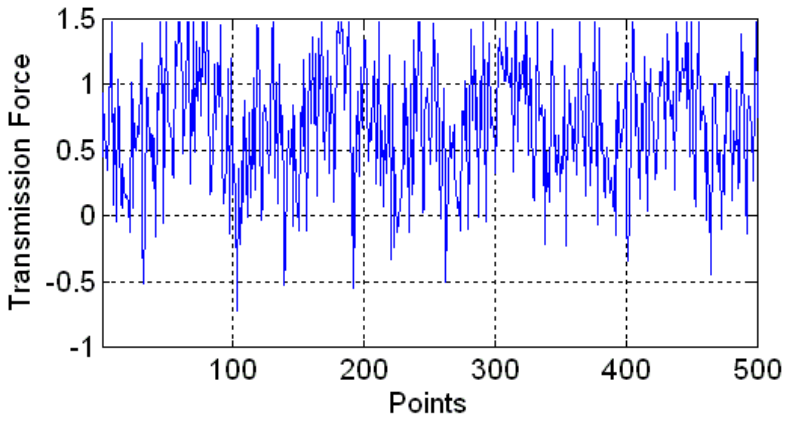

(b)

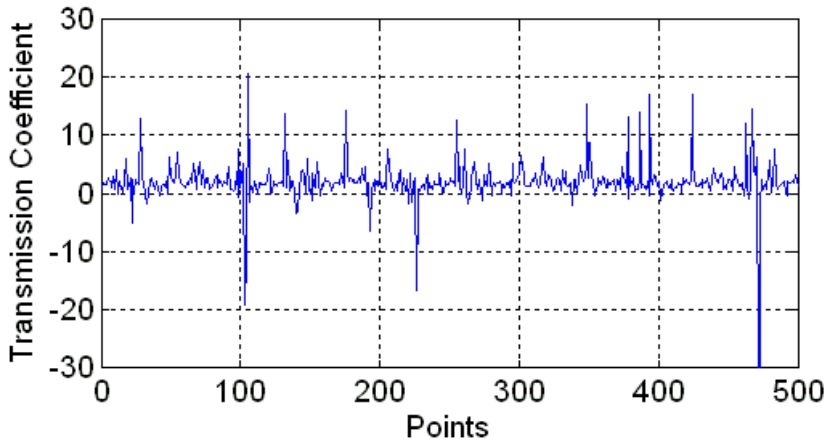

(c)

Fig. 8 A typical set of raw time series data obtained from the friction apparatus: (a) loading force, (b) transmission (drag) force, and (c) the instantaneous transmission coefficient.

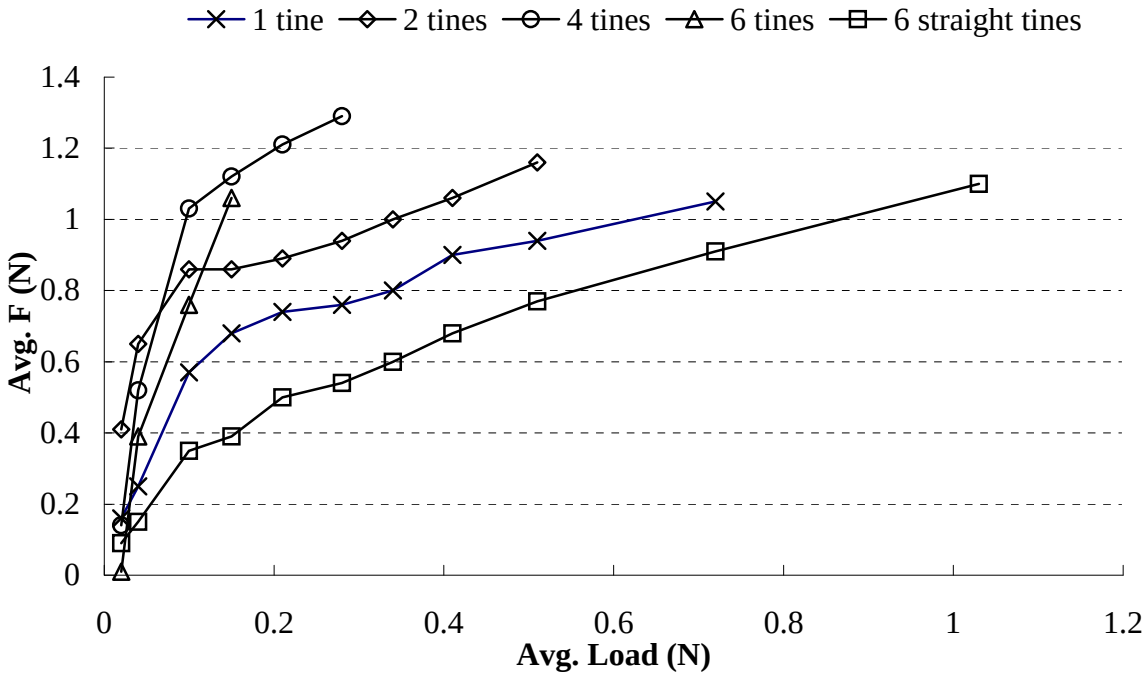

Fig. 9 The average transmission force as a function of the average loading force

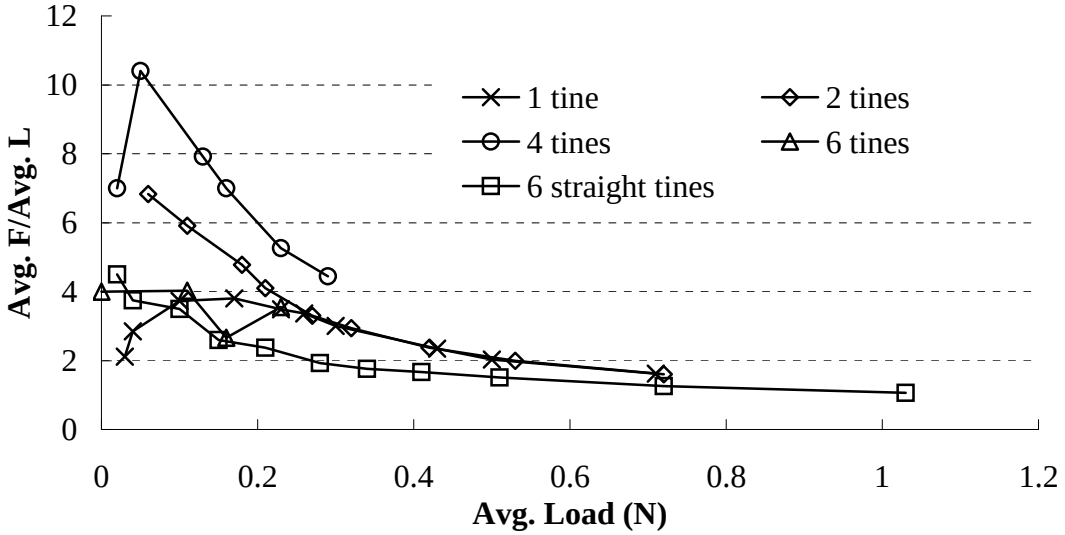

(a)

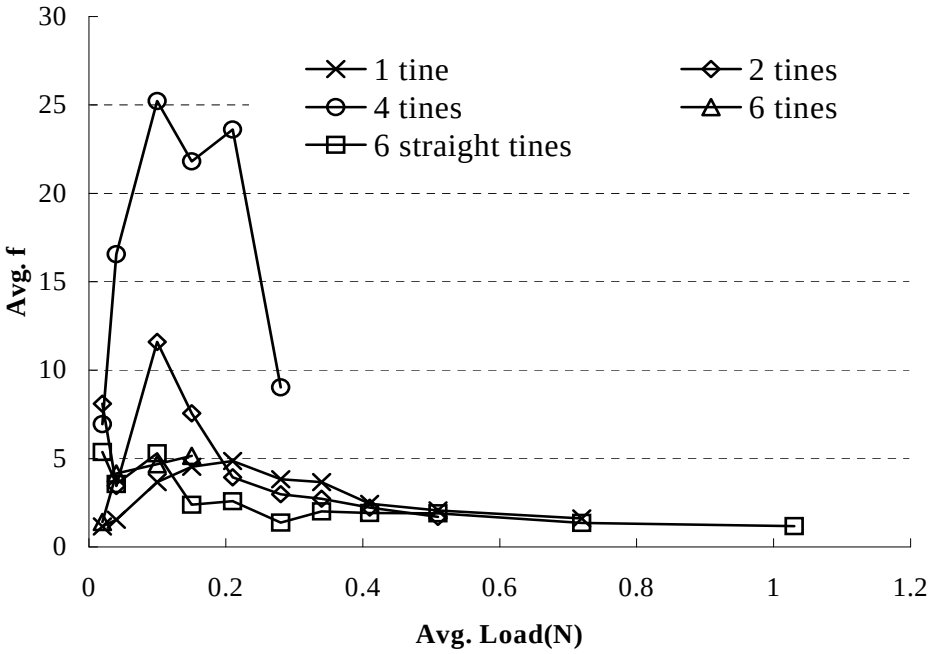

(b)

Fig. 10 Transmission coefficients as a function of averaged loading force: (a) averaged transmission coefficient (ratio of time averaged forces), and (b) time average of instantaneous transmission coefficient after removal of outliers.

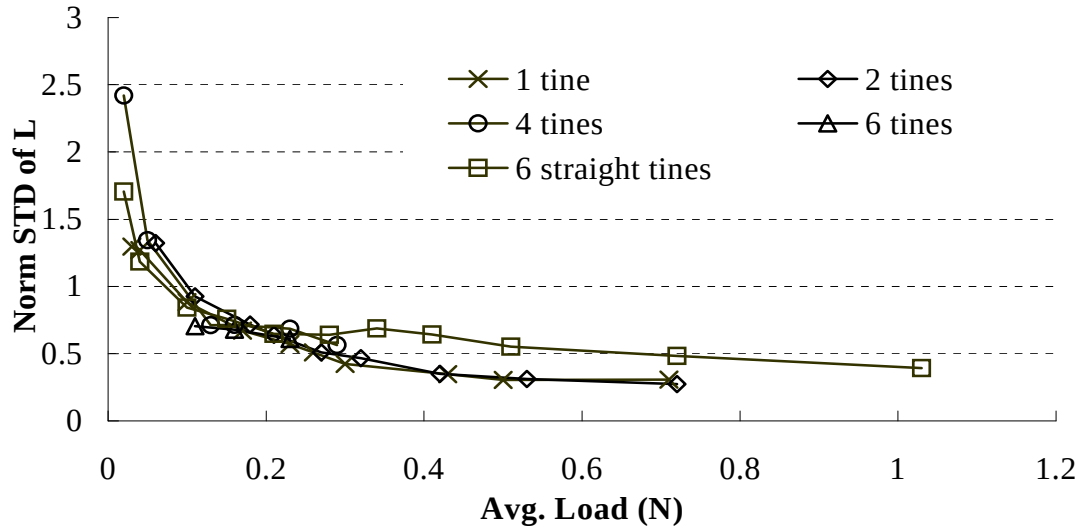

(a)

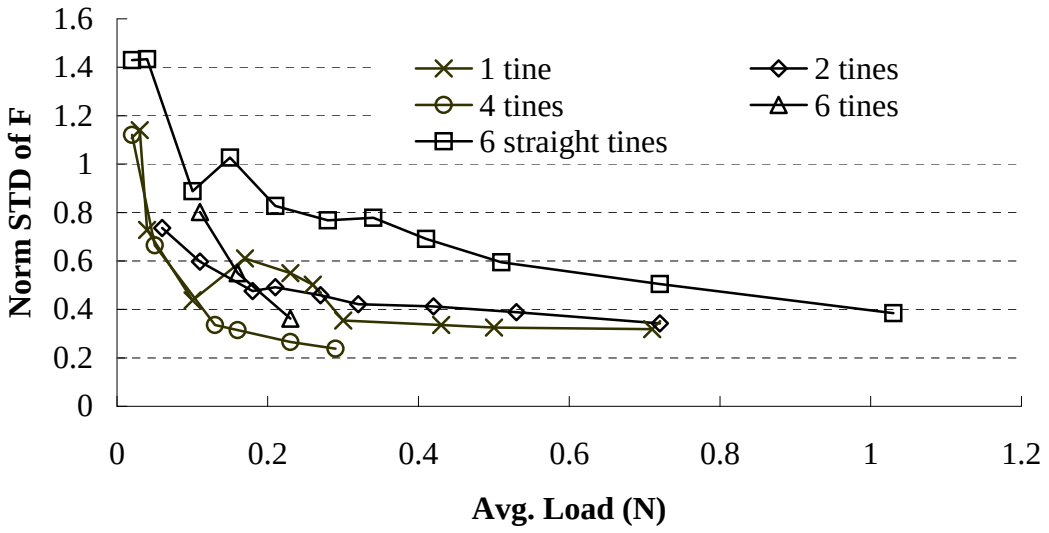

(b)

Fig. 11 Normalised standard deviation of (a) loading force and (b) transmission force as a function of averaged loading force.

Table 1 Parameters of Velcro® surfaces used for different type 1specimens.

Arrangement	Tines per row	Tine height, *h*, (mm)	Surface width,B, (mm)
1 tine	1	1.5	1.5
1×2 tines	2	1.5	2.0
2×2 tines	4	1.5	3.0
3×2 tines	6	1.5	4.5
3×2 straight tines	6	1.0	4.5

Table 2 Comparison of transmission forces for hooked tines estimated from experimental data in Fig. 8 and from predictions using Eq. (12). Values in brackets are extrapolations.

N_R	Source	F_L = 0.2 N	F_L = 0.4 N	F_L = 0.8 N
1	Model: p = 1.0; μ = 0.7	0.67 N	0.81 N	1.09 N
	Experimental	0.7 N	0.9 N	(1.1 N)
2	Model: p = 0.7; μ = 0.6	0.86 N	0.98 N	1.22 N
	Experimental	0.85 N	1.0 N	1.2 N
4	Model: p = 0.5; μ = 0.65	1.19 N	1.32 N	1.58 N
	Experimental	1.15 N	1.4 N	(1.55 N)